

# Parahydrogen Cooling of Nuclear Spin Chains at Hypogeomagnetic Fields

Alexey Kiryutin<sup>1,2</sup>, Danil Markelov<sup>3</sup>, Ivan Zhukov<sup>1,2</sup>, Erik Van Dyke<sup>4,5,6</sup>, Alexandra Yurkovskaya<sup>1,2</sup>, and Danila Barskiy<sup>\*7,8,9</sup>

<sup>1</sup>*International Tomography Center, SB RAS, Novosibirsk, Russia*

<sup>2</sup>*Novosibirsk State University, Novosibirsk, Russia*

<sup>3</sup>*Chimie Physique et Chimie du Vivant (CPCV, UMR 8228), Département de Chimie, École Normale Supérieure, PSL University, Sorbonne Université, Paris 75005, France*

<sup>4</sup>*Johannes Gutenberg University, Institute of Physics, 55128 Mainz, Germany*

<sup>5</sup>*Helmholtz Institute Mainz, 55099 Mainz, Germany*

<sup>6</sup>*GSI Helmholtzzentrum für Schwerionenforschung GmbH, 64291 Darmstadt, Germany*

<sup>7</sup>*Department of Chemistry, University of Miami, Coral Gables, FL 33146, USA*

<sup>8</sup>*Department of Physics, University of Miami, Coral Gables, FL 33146, USA*

<sup>9</sup>*Frost Institute for Chemistry and Molecular Science, Coral Gables, FL 33146, USA*

## Abstract

Solution-state molecular nuclear spin networks are promising quantum simulators because their scalar-coupling Hamiltonians are chemically programmable, precisely measurable, and coherent at room temperature. Their main limitation for quantum information science is initialization: thermal Boltzmann polarization produces highly mixed, high-entropy states. Here,<sup>1</sup> we use parahydrogen-based Signal Amplification by Reversible Exchange (SABRE) at hypogeomagnetic fields (i.e., magnetic fields below Earth field) to hyperpolarize the chemically engineered 12-spin chain [U-<sup>13</sup>C,<sup>15</sup>N]-butyronitrile. SABRE generates percent-level <sup>13</sup>C and <sup>15</sup>N polarization and prepares non-equilibrium multi-spin orders across the network. A von Neumann entropy analysis of such a hyperpolarized system shows that, at the optimal transfer field of 0.52  $\mu$ T, the full spin system could reach  $S/k_B = 8.274$ , compared with  $S_{\text{th}}/k_B = 8.318$  for the unpolarized reference, giving  $(S - S_{\text{th}})/k_B = -0.043$ . Experimentally, nuclear spin temperatures of 52 mK and 257 mK are achieved for <sup>15</sup>N and <sup>13</sup>C subensembles, respectively. The larger entropy deficit of the full network than of individual subsystems indicates correlated multi-spin order beyond single-spin polarizations. Rapid field cycling to 9.4 T enables site-resolved NMR readout, while the precisely determined coupling network provides an experimentally benchmarked Hamiltonian for testing quantum-simulation, quantum-control, and Hamiltonian-learning protocols.

**Keywords:** Nuclear magnetic resonance; hyperpolarization; parahydrogen; hypogeomagnetic fields; zero-to-ultralow fields; SABRE; spin chains;  $J$ -couplings; Heisenberg Hamiltonians; quantum simulations

---

\*To whom correspondence should be addressed. E-mail: barskiy@miami.edu

<sup>1</sup>This article is based on discussions and experiments conducted before February 2022.

# Introduction

Quantum computation promises to outperform classical approaches in a variety of tasks ranging from integer factorization in cryptography [1, 2] to the simulation of complex molecular and quantum many-body systems [3–6]. Among the physical platforms explored for implementing quantum information processing, nuclear magnetic resonance (NMR) has historically played an important role as a testbed for small-scale quantum algorithms [7–11]. Early demonstrations, including implementations of Shor’s factoring algorithm [12] and Grover’s search [13], showed that coupled networks of nuclear spins can serve as controllable quantum registers, where radiofrequency pulse sequences implement unitary operations and NMR spectra provide direct readout of statistically averaged quantum states [14]. Carefully designed pulse sequences allow the engineering of effective Hamiltonians and high-fidelity quantum gates [15–22], which have enabled a wide range of proof-of-principle experiments demonstrating coherent control of multi-spin systems [23, 24].

Individual nuclear spins are natural qubits, with scalar  $J$ -couplings mediating interactions necessary for multi-qubit operations. These couplings also facilitate the propagation of quantum correlations and the transfer of spin order along the network [25, 26]. Nuclear spins are particularly attractive for such studies because their  $J$ -coupling constants are well characterized and coherence times can remain long ( $T_2^* \gg 1/J$ ) even at room temperature. One particularly interesting realization of nuclear spin networks are one-dimensional spin chains, which, in practice, can be realized by using molecules in solution [26–30]. They provide controllable and chemically tunable platforms for exploring quantum transport, entanglement growth, and many-body spin dynamics in chemically and biologically relevant environments.

While molecular spin chains offer a versatile framework for studying quantum dynamics, a fundamental limitation of conventional liquid-state NMR quantum computing arises: thermal equilibrium polarization of nuclear spins is extremely small, typically not exceeding 0.001–0.01%. Therefore, the initial state of such spin ensemble is highly mixed, and most implementations to date have relied on the so-called pseudo-pure states that emulate pure-state quantum computation within a largely unpolarized spin ensemble [31–35]. Although this approach has enabled pioneering demonstrations of quantum algorithms, the exponentially decreasing purity with system size severely limits scalability [36].

Hyperpolarization methods offer a promising route for overcoming intrinsically low thermal polarization in NMR. Several techniques enable nuclear spin polarization to  $\gtrsim 10\%$  [37, 38], therefore, potentially providing the critical state-preparation resource to increase the initial state purity often required for quantum computing and quantum simulations [36, 39–41]. In particular, the enhanced polarization allows the preparation of highly ordered initial states (pre-initialization) of interacting nuclear spins. The degree of such spin ordering can be quantified thermodynamically through the spin system entropy: lower value corresponds to a more ordered nuclear spin ensemble. For Zeeman-polarized spin subsystems, the same non-equilibrium order can also be expressed as an effective spin temperature, providing an intuitive metric for how far the nuclear spin populations have been driven from room-temperature Boltzmann equilibrium. Importantly, pre-initialization does not need to cool the sample itself, but it should reduce the entropy and effective spin temperature of the nuclear spin degrees of freedom. Although the ensembles can remain mixed, the substantially increased polarization and the presence of multispin orders are expected to be readily employed for preparing pseudo-pure states via pulse sequences/adiabatic protocols, facilitating the development of experiments with nuclear-based multispin registers applicable toward a wider range of problems compared to previously conducted liquid-state-NMR-based demonstrations [42].

Among hyperpolarization strategies, parahydrogen provides a particularly attractive source of nuclear spin order for quantum initialization [43–46]. Parahydrogen ( $p\text{H}_2$ ) is the singlet nuclear-spin

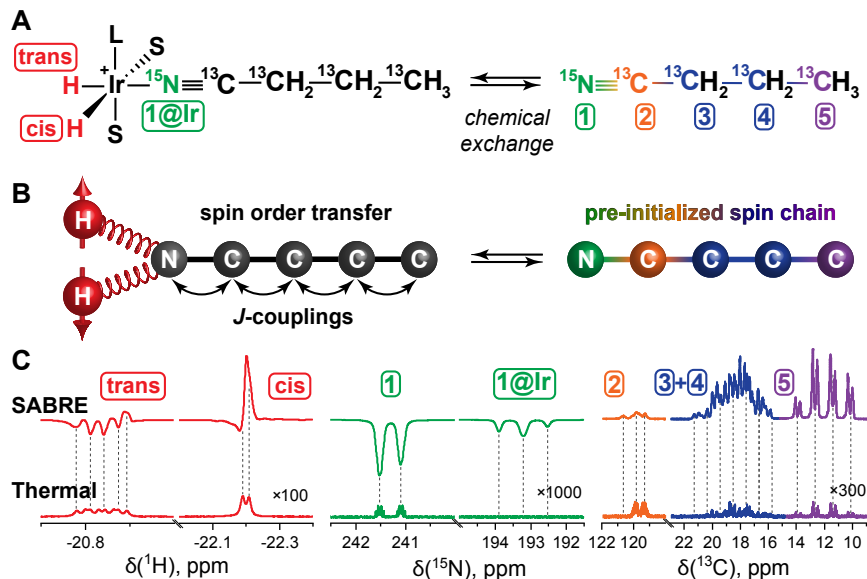


Figure 1: Signal Amplification by Reversible Exchange (SABRE) as a method for pre-initializing nuclear spin chains. (A) Schematic of the reversible exchange of parahydrogen and a  $[\text{U}-^{13}\text{C}, ^{15}\text{N}]$ -butyronitrile spin chain with an Ir-based polarization transfer complex. L and S denote ancillary ligands of the complex. (B) Polarization transfer from parahydrogen to the spin chain occurs through the network of scalar  $J$ -couplings within the complex, resulting in hyperpolarization of the spin chain. (C)  $^1\text{H}$ ,  $^{15}\text{N}$ , and  $^{13}\text{C}$  NMR signals hyperpolarized by SABRE at  $1 \mu\text{T}$  (top traces) compared with the corresponding thermal spectra, scaled by factors of 100, 1000, and 300, respectively (bottom traces). Note that some signals (e.g., 1@Ir) in the top SABRE-polarized spectra correspond to the Ir-complex-bound spin chain molecules.

isomer of the  $\text{H}_2$  molecule, prepared by cooling the gas to cryogenic temperatures in the presence of paramagnetic catalysts ( $\sim 25 \text{ K}$ ). Although NMR-silent, this singlet spin order can be converted into observable nuclear polarization in the products of  $p\text{H}_2$  addition reactions. The resulting polarization corresponds to an effective spin temperature of as low as 6.4 mK, making parahydrogen-derived spin order a highly non-equilibrium resource for quantum information processing [47]. Although the idea of using  $p\text{H}_2$  as a source of quantum state initialization is not new, it has only been demonstrated on a two-atom system of a metal hydride without subsequent polarization transfer. In this work, we extend the scope of quantum pre-initialization from two to 12 spins by using an exemplary nuclear spin chain system with a well defined coupling network [26].

Signal Amplification by Reversible Exchange (SABRE) is a  $p\text{H}_2$ -based hyperpolarization technique that has emerged as a particularly versatile approach for generating substantial nuclear polarization [48, 49]. In SABRE, spin order from  $p\text{H}_2$  is transferred to the target nuclei via reversible exchange with a metal complex, producing hyperpolarization without modifying the substrate chemically; because the exchange cycle is reversible, hyperpolarization can be regenerated continuously as long as fresh  $p\text{H}_2$  is supplied. Under hypogeomagnetic (microtesla) magnetic fields, strong mixing of spin states allows efficient propagation of polarization from  $p\text{H}_2$  to heteronuclei through the network of scalar couplings, distributing it across multiple spins [50, 51]. The coherent nature of this transfer has been directly observed via oscillatory polarization dynamics when passing through level anti-crossings (LACs) in model three-spin systems [52], confirming that interactions with  $p\text{H}_2$  can establish correlated multispin orders rather than merely independent polarizations.

This ability to channel polarization along coupled-spin networks as well as ease with which multiple experiments can be repeated on the same sample, makes SABRE especially well suited for preparing highly spin-ordered nuclear spin chains at room temperature. Such spin chains are poised to become fruitful platforms for quantum information simulation/processing experiments as well as artificial intelligence-enhanced quantum simulation approaches [53].

In this work, we employ SABRE to hyperpolarize nuclear spin chain [U- $^{13}\text{C}$ ,  $^{15}\text{N}$ ]-butyronitrile, generating enhanced and distributed polarization across a network of coupled nuclear spins. This effectively corresponds to spin cooling down to  $\sim 50$  mK, albeit the chemical system remains at steady state and room temperature. The capacity of SABRE to hyperpolarize multiple spins simultaneously provides a route to preparing spin ensembles for quantum information processing and quantum simulation in liquid-state NMR. Rather than implementing a specific algorithm, the goal of this work is to establish a valid method for pre-initializing (beyond Boltzmann polarization) multi-spin registers that can serve as platforms for quantum control and computation experiments. SABRE-generated polarization produces pre-initialization, i.e., multi-spin states with substantially higher purity than conventional thermal equilibrium states, bringing them closer to the ideal initial states required in quantum information processing. Our approach opens the doors to exploring larger highly polarized spin networks, expanding the experimental capabilities of NMR-based quantum information science.

## Results

Figure 1 schematically introduces the SABRE-based pre-initialization scheme used in this work. Reversible exchange of  $p\text{H}_2$  and [U- $^{13}\text{C}$ ,  $^{15}\text{N}$ ]-butyronitrile on the Ir-based polarization-transfer complex (with L denoting IMes = 1,3-bis(2,4,6-trimethylphenyl)-1,3-dihydro-2H-imidazol-2-ylidene, and S denoting pyridine as the ancillary ligand) together with coherent transfer of spin order from the ligated  $p\text{H}_2$  atoms results in the accumulation of polarization on the free spin-chain molecules (Fig. 1A). Through the  $J$ -coupling network, this process prepares ordered states of the coupled nuclear-spin ensemble in the bulk sense [31]. Importantly, SABRE polarizes all nuclei in the molecule simultaneously [54], and the specific spin orders that are created depend on the magnetic field at which polarization transfer takes place as well as on the field manipulations applied during the experiment (Fig. 1B) [55–57].

Representative SABRE-polarized and thermally polarized  $^1\text{H}$  (hydride region),  $^{15}\text{N}$ , and  $^{13}\text{C}$  NMR spectra are shown in Fig. 1C. The upper traces correspond to SABRE-enhanced signals obtained at a transfer field of  $1 \mu\text{T}$ , whereas the lower traces show the corresponding thermal spectra scaled by factors of 100, 1000, and 300, respectively. After only a few seconds of  $p\text{H}_2$  bubbling through the solution, SABRE yields signal enhancements ranging from several hundred to a few thousand. In addition to signals from free [U- $^{13}\text{C}$ ,  $^{15}\text{N}$ ]-butyronitrile, the SABRE spectra also contain contributions from bound spin-chain molecules: for example, “1@Ir” denotes the nitrile  $^{15}\text{N}$  atom bound to the polarization-transfer complex, and additional bound-state peaks are also observed for some carbon atoms (e.g., for  $\text{C}_2$ ).

The line shapes in the  $^{15}\text{N}$  NMR spectra reflect the coupling topology of the spin system. The  $^{15}\text{N}$  signal of free [U- $^{13}\text{C}$ ,  $^{15}\text{N}$ ]-butyronitrile appears as a doublet because the nitrile  $^{15}\text{N}$  is split by the directly bonded  $^{13}\text{C}$  (17.37 Hz). By contrast, the corresponding signal of the bound spin-chain molecule (1@Ir) appears as a triplet. This pattern arises from the combined action of the  $^{15}\text{N}$ - $^{13}\text{C}$  coupling within the nitrile group and the coupling to the trans-hydride in the Ir complex (see Supporting Information, SI, for details). Because the  $^{15}\text{N}$ - $^1\text{H}$  and  $^{15}\text{N}$ - $^{13}\text{C}$  couplings are of similar magnitude ( $J_{\text{NH}} = -25.6$  Hz,  $J_{\text{NC}} = 30.3$  Hz), the resulting multiplet appears triplet-like.

Figure 2 compares SABRE-enhanced  $^{15}\text{N}$  and  $^{13}\text{C}$  NMR spectra recorded after  $p\text{H}_2$  bubbling at ultralow magnetic fields, between  $-0.5 \mu\text{T}$  and  $+0.9 \mu\text{T}$ , where the sign indicates the field direction relative to the detection field of the high-field NMR spectrometer. For both types of nuclei,  $^{15}\text{N}$  and  $^{13}\text{C}$ , the spectra display strongly enhanced lines with both positive and negative contributions, indicating the formation of various multispin orders in the chain molecule.

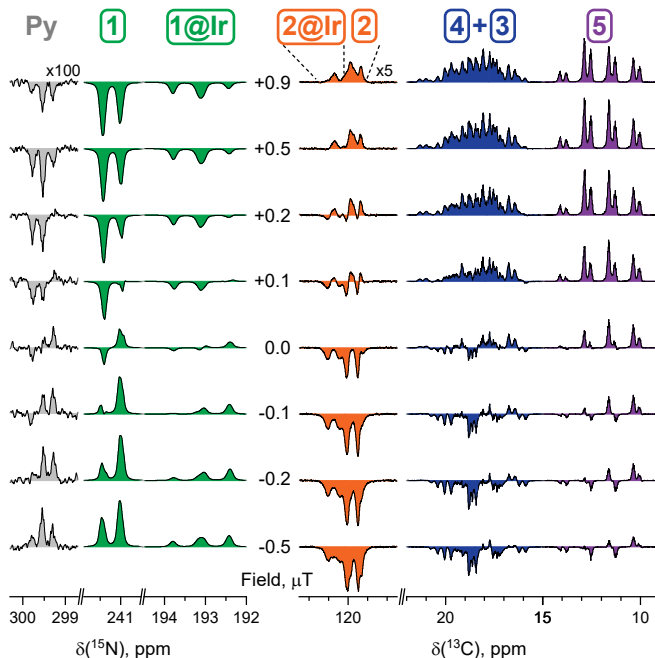


Figure 2:  $^{15}\text{N}$  (left) and  $^{13}\text{C}$  (right) NMR spectra (9.4 T) of  $[\text{U-}^{13}\text{C}, ^{15}\text{N}]$ -butyronitrile obtained after SABRE polarization at ultralow magnetic fields (from  $-0.5 \mu\text{T}$  to  $+0.9 \mu\text{T}$ ). The negative sign of the magnetic field indicates the opposite direction relative to the detection field in the NMR magnet. Note the multiplication factors of  $\times 100$  and  $\times 5$  for the data columns corresponding to pyridine (Py) and 2@Ir/2, respectively.

The intensities of the individual  $^{15}\text{N}$  lines strongly depend on the polarization-transfer field. At zero magnetic field,  $^{15}\text{N}$  NMR spectra consist of antiphase multiplets, such that the total integral of each multiplet is close to zero. The same qualitative behavior is observed for pyridine (Fig. 2, left), which serves as a co-ligand to stabilize metal complex (Ir complex with only butyronitrile ligands is unstable).  $^{15}\text{N}$  NMR signal of pyridine (nat. abun.) appears as a triplet because of splitting by the two equivalent ortho-protons in the aromatic ring. Overall, the sign of the  $^{15}\text{N}$  polarization changes approximately symmetrically around zero field.

The  $^{13}\text{C}$  NMR spectra behave differently. Unlike the response of the  $^{15}\text{N}$  spins, the  $^{13}\text{C}$  spectra display a pronounced asymmetry with respect to the sign of the applied transfer field. This asymmetry is not a property of our SABRE step; rather, it reflects polarization/spin order redistribution among the carbon spins during sample transfer from the field at which  $p\text{H}_2$  is introduced into the system to the high-field NMR spectrometer. Although both coherent transfer through the  $J$ -coupling network and incoherent cross-relaxation may occur, the dominant contribution is expected to be coherent [26]. It is during this transport stage ( $\approx 400$  ms) that redistribution of non-equilibrium polarizations occurs among spins of the same type (e.g.,  $\text{C}_2$ - $\text{C}_5$ ) due to the strong coupling in field regimes ranging from  $\mu\text{T}$  to mT. This effect is analogous to the well known AL-TADENA experiment [26, 58], in which the two outermost NMR lines of a coupled spin system

acquire strongly enhanced polarizations of opposite sign, so that one end of the spectrum appears positive and the other negative [59, 60]. The contrast between pyridine and the spin chain shows that the dynamics of the spin chain molecule are exceptionally sensitive to tiny magnetic fields, those that even NMR features of SABRE-polarized [ $^{15}\text{N}$ ]-pyridine cannot capture.

Figure 3A directly summarizes the field dependence of SABRE polarization in the ultralow-field range from  $-4\ \mu\text{T}$  to  $+4\ \mu\text{T}$ , where states of different spin types ( $^{15}\text{N}$ ,  $^{13}\text{C}$ , and  $^1\text{H}$ ) mix. In the upper part of the panel, the experimental signal intensities obtained after 10 s of  $p\text{H}_2$  bubbling at  $25^\circ\text{C}$  are plotted as a function of the transfer field. The intensities are reported as percentages of the maximum theoretical polarization. For the  $^{15}\text{N}$  spin, the field dependence is an odd function of the magnetic field, implying that the integrated signal of 1 and 1@Ir vanishes at zero field, and the polarization reaches a maximum at about  $2\ \mu\text{T}$ . The  $^{13}\text{C}$  spins also show a maximum, but at a lower field of about  $0.5\ \mu\text{T}$ .

The lower part of Fig. 3A shows the corresponding theoretical SABRE calculation, which includes all spins but assumes instantaneous field switching. For the  $^{15}\text{N}$  spin, the calculation reproduces the antisymmetry about zero field very well and predicts the polarization maximum at  $1\text{--}2\ \mu\text{T}$ . For the carbon spins, it captures the overall field dependence and the position of the SABRE maximum reasonably well, but clear discrepancies remain. In the calculation,  $\text{C}_2$  has the highest polarization among the  $^{13}\text{C}$  nuclei, whereas experimentally it has the lowest. In contrast, the distant chain spin  $\text{C}_5$  is only weakly polarized in the calculation but shows the strongest experimental enhancement, consistent with the spectra in Fig. 2 (note the multiplication factor of 5 for all “2/2@Ir” NMR spectra). The calculation also fails to reproduce the asymmetry of the  $^{13}\text{C}$  signals about zero field. Both discrepancies likely arise from the experimental field-switching protocol: after a rapid electromagnetic switch to  $50\ \mu\text{T}$ , the sample is moved out of the magnetic shield, and during this slower second stage the field increases smoothly from  $50\ \mu\text{T}$  to the detection field of  $9.4\ \text{T}$ . During this  $\approx 400\ \text{ms}$  interval, coherent redistribution of non-equilibrium polarization can occur among spins of the same type (e.g.,  $\text{C}_2\text{--}\text{C}_5$ ) because of strong coupling in the  $\mu\text{T}$ -to-mT range, altering the observable signal intensities compared to those expected from the sudden-switch experiments.

Figure 3B shows the buildup of SABRE polarization in [ $\text{U}\text{-}^{13}\text{C},^{15}\text{N}$ ]-butyronitrile at two representative transfer fields,  $0.4$  and  $2.0\ \mu\text{T}$ . The thin black lines are mono-exponential fits used to extract the effective buildup time constant,  $\tau_{\text{eff}}$ . The growth of  $^{15}\text{N}$  polarization is well described by a mono-exponential function, yielding time constants of  $2.5\ \text{s}$  and  $3.8\ \text{s}$  at  $0.4\ \mu\text{T}$  and  $2.0\ \mu\text{T}$ , respectively. The buildup is much faster than the high-field relaxation times of  $^{15}\text{N}$  and  $^{13}\text{C}$  and is therefore expected to be governed by the collective relaxation dynamics of the coupled butyronitrile spin system while the molecule is bound to the iridium complex. This field dependence of the buildup time should be carefully considered in other SABRE experiments that map polarization as a function of the transfer field, for example when  $p\text{H}_2$  is bubbled continuously while the magnetic field is varied. If a single buildup time optimized for one field is used across the entire field profile, polarization at other fields may not have reached its plateau, leading to an apparent field dependence that reflects incomplete buildup rather than the true SABRE transfer efficiency at a given field.

The lower panel of Fig. 3B shows the corresponding buildup of  $^{13}\text{C}$  polarization. In contrast to the  $^{15}\text{N}$  case, the  $^{13}\text{C}$  buildup at  $2.0\ \mu\text{T}$  exhibits a pronounced slow initial phase, indicating that the polarization dynamics are not purely mono-exponential but are shaped by subsequent redistribution through the  $J$ -coupling network. Together, Figs. 3A and 3B provide a compact description of the field dependence and buildup dynamics of SABRE polarization in this spin-chain system.

## Discussion

We calculated the von Neumann entropy,  $S = -k_B \text{Tr}(\hat{\rho} \ln \hat{\rho})$ , for the nuclear spin chain across a range of magnetic fields at which SABRE polarization transfer takes place (here,  $\hat{\rho}$  is a density matrix of [U- $^{13}\text{C}$ , $^{15}\text{N}$ ]-butyronitrile and  $k_B$  is the Boltzmann’s constant). The reference state was taken as the completely unpolarized ensemble, neglecting the thermal polarization at room temperature [61]. The entropy was evaluated for the four cases: the full spin system (all  $^1\text{H}$ ,  $^{13}\text{C}$ , and  $^{15}\text{N}$  nuclei), the heteronuclear subsystem ( $^{13}\text{C}$  and  $^{15}\text{N}$  only), the carbon subsystem ( $^{13}\text{C}$  spins only), and the nitrogen subsystem ( $^{15}\text{N}$  only), as shown in Table 1. The largest deviation of the entropy from thermal equilibrium,  $(S - S_{\text{th}})/k_B = -4.3 \times 10^{-2}$ , was observed for the whole system at the magnetic field of  $0.52 \mu\text{T}$ , which coincides with the numerically calculated maximum of  $^{15}\text{N}$  and  $^{13}\text{C}$  polarization, as shown in Fig. 3A. Notably, this deviation is greater than that of any individual spin subsystem, indicating the efficient generation of not only polarization but also of multi-spin correlations among  $^{15}\text{N}$ ,  $^{13}\text{C}$ , and  $^1\text{H}$  nuclei (see Fig. S1). This result demonstrates that SABRE methodology significantly reduces the entropy of the spin chain, driving the system toward a more ordered state, pre-initialized for subsequent quantum information protocols. For reference, thermal polarization of the same spin system at 9.4 T reduces the entropy relative to the fully unpolarized state by merely  $10^{-9}$ . The SABRE-induced entropy reduction therefore exceeds this value by more than seven orders of magnitude, demonstrating the remarkable capability of SABRE to create highly ordered spin states, in a few seconds and at room temperature.

Table 1: Deviations of [ $^{13}\text{C}$ , $^{15}\text{N}$ ]-butyronitrile’s spin entropy from thermal equilibrium and effective spin temperatures at 10 T corresponding to the SABRE pre-initialization field of  $0.52 \mu\text{T}$ .

Spin system	$S/k_B$	$S_{\text{th}}/k_B$	$(S - S_{\text{th}})/k_B \times 10^2$	$T_E$ , mK
Full (12 spins)	8.274	8.318	-4.3	—
$^{15}\text{N}$ , $^{13}\text{C}$ (5 spins)	3.438	3.466	-2.7	—
$^{15}\text{N}$ (1 spin)	0.680	0.693	-1.3	52
$^{13}\text{C}$ (4 spins)	2.762	2.773	-1.1	257

$k_B = 1.38 \times 10^{-23}$  [J/K] is the Boltzmann constant;  
 $S_{\text{th}} = N k_B \ln 2$  is the entropy for  $N$  unpolarized spin-1/2 nuclei;  $T_E$  is experimentally measured spin temperature.

If all available spin orders were to transfer into a single transition, i.e., corresponding to  $^{15}\text{N}$  spin flips, Sørensen bounds can give an estimate [62]. We concluded that a pulse sequence/adiabatic protocol with rational design could therefore improve the achieved signal intensities and also produce an appropriate initial state with a substantial purity of  $\sim 15\%$  (see SI).

Because the spin system evolves under a fully characterized spin-coupling Hamiltonian, the experiment directly implements analog quantum simulation of a Heisenberg spin chain: measured time-domain observables provide ground-truth dynamics that can be compared against classical calculations and, in future work, against quantum algorithms attempting to reproduce the same evolution under experimentally realistic control constraints.

More broadly, the combination of zero- to ultralow-field (ZULF) evolution with high-field detection cleanly separates Hamiltonian dynamics from site-resolved readout. In the ZULF regime, chemical-shift dispersion is quenched and the isotropic scalar-coupling Hamiltonian is not truncated by dominant Zeeman terms, enabling strong heteronuclear couplings and Heisenberg-type dynamics. High-field readout then restores both sensitivity and chemical-shift resolution, allowing site-specific spectral assignment. Magnetic field cycling therefore provides a practical interface between an analog many-body simulator and a conventional high-field NMR measurement layer.

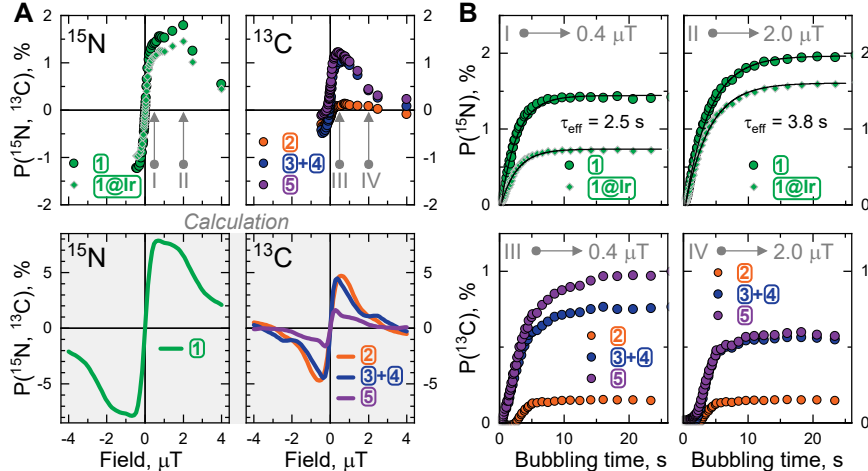


Figure 3: (A) Experimental (top) and calculated (bottom) dependence of signal intensities of SABRE-polarized signals as a function of ultralow magnetic field during parahydrogen bubbling. The bubbling time was set to 10 s for all experiments, and the temperature was maintained at 25 °C; (B) Dynamics of SABRE polarization buildup measured at magnetic fields of 0.4  $\mu\text{T}$  and 2.0  $\mu\text{T}$  for the  $^{15}\text{N}$  (top) and  $^{13}\text{C}$  (bottom) spins in  $[\text{U-}^{13}\text{C}, ^{15}\text{N}]$ -butyronitrile. All signal intensities are given as a percentage of the maximum theoretical polarization. The thin black lines show fits to the data using a mono-exponential function with the effective buildup time constant,  $\tau_{\text{eff}}$ .

The same pre-initialization can also be expressed in terms of an effective Zeeman spin temperature,  $T_E$ . For a spin-1/2 nucleus with polarization  $P$  in a magnetic field of magnitude  $B$ , inversion of the Boltzmann relation gives  $T_E = |\hbar\gamma B / (2k_B \text{arctanh}(P))|$ . Using  $|\gamma_{^{15}\text{N}}|/2\pi = 4.316 \text{ MHz T}^{-1}$ , a  $^{15}\text{N}$  polarization of 20% at  $\simeq 10 \text{ T}$  corresponds to  $\simeq 5 \text{ mK}$ . At the SABRE transfer field, the same thermometric scale becomes dramatically more stringent: achieving even 1% thermal  $^{15}\text{N}$  polarization at 0.5  $\mu\text{T}$  would require  $\simeq 5 \text{ nK}$ . For comparison, the lowest artificial matter temperature reported to date, 38 pK [63], would correspond to  $P_{^{15}\text{N}} \simeq 88\%$  at 0.5  $\mu\text{T}$ . These estimates emphasize that SABRE does not cool the liquid sample itself; rather, it prepares a room-temperature ensemble whose nuclear Zeeman populations, multispin correlations, and von Neumann entropy correspond to a spin reservoir far outside the range accessible by ordinary Boltzmann polarization. To our knowledge, such a quantitative entropy and spin-temperature assignment for SABRE-pre-initialized, liquid-state molecular spin-chain registers has not previously been reported.

A natural next step is to convert SABRE-prepared, lower-entropy spin ensembles into targeted initial states for quantum-simulation and quantum-control experiments. The present platform already provides a useful set of native operations: magnetic-field quenches between weak- and strong-coupling regimes, evolution under the intrinsic isotropic  $J$ -coupling Hamiltonian at ZULF, global DC control at ultralow field, selective RF control and site-resolved detection at high field, and hyperpolarized pre-initialization from  $p\text{H}_2$ . Together with an independently benchmarked coupling network, these capabilities make the system well suited for algorithm–hardware co-design, where pulse sequences, field-cycling trajectories, and state-preparation protocols are optimized for the experimentally available operations rather than imposed from an idealized gate model.

Such calibrated molecular spin chains can therefore serve as compact, reproducible testbeds for near-term quantum science. They provide experimentally accessible examples in which the Hamiltonian is known, the initial state can be driven far beyond thermal Boltzmann polarization, and the resulting dynamics can be measured with high spectral resolution. This combination is

valuable for validating Hamiltonian-learning methods [64], benchmarking time-evolution algorithms [65, 66], testing strategies for generating and detecting multispin correlations [67, 68], and exploring how non-equilibrium spin order propagates through chemically defined networks [69]. Because the molecular scaffold can be varied synthetically, the same approach can be extended to spin chains with different lengths, topologies, coupling strengths, and relaxation environments.

Overall, this work establishes parahydrogen-driven SABRE hyperpolarization at hypogeomagnetic (i.e., ZULF) fields as a practical route for pre-initializing molecular nuclear spin chains. In [U- $^{13}\text{C}$ ,  $^{15}\text{N}$ ]-butyronitrile, SABRE produces percent-level heteronuclear polarization, creates correlated multispin order, and measurably reduces the entropy of a 12-spin network within seconds at room temperature. By combining this beyond-Boltzmann initialization with field-cycling control and high-field NMR readout, the approach bridges hyperpolarization chemistry, precision spectroscopy, and quantum simulation. These developments point toward increasingly capable liquid-state NMR platforms in which chemically programmable molecules act as calibrated, hyperpolarized quantum simulators for studying coherent spin dynamics in realistic many-spin systems.

## Materials and Methods

### NMR Experiments

NMR experiments were performed using a home-built mechanical field-cycling setup based on a 400 MHz NMR spectrometer, equipped with a magnetic field shield installed on top of the cryomagnet [70]. This versatile setup enables both magnetic field cycling and in-situ sample bubbling with parahydrogen under elevated pressure across a wide range of magnetic fields [71]. High-resolution NMR spectra for spin system simulation were acquired on a separate NMR spectrometer with a base proton frequency of 700 MHz at ambient temperature.

As a source of non-thermal polarization, we utilized parahydrogen gas (85% enrichment, Bruker parahydrogen generator BPHG-90) in the Signal Amplification By Reversible Exchange (SABRE) process. The solution for SABRE experiments contained 12.9 mM of [U- $^{13}\text{C}$ ,  $^{15}\text{N}$ ]-butyronitrile, 20 mM of  $^{14}\text{N}$ -pyridine as a co-ligand, and 5.3 mM of the precatalyst [IrCl(COD)(IMes)] in deuterated methanol- $d_4$ . To activate the precatalyst by hydrogenation of cyclooctadiene (COD) and form the stable iridium complex with pyridine and butyronitrile, the solution was purged with parahydrogen gas at 3 bar for approximately 15 minutes. SABRE experiments were performed at 20 °C with a bubbling time of 10 seconds using the aforementioned field-cycling apparatus. The setup includes an add-on for in-situ bubbling in a standard NMR sample tube at elevated pressures up to 10 bars; further details of this apparatus can be found in references [71, 72].

### *J*-coupling determination by fitting of NMR spectra

$^1\text{H}$ ,  $^{13}\text{C}$ , and  $^{15}\text{N}$  high resolution NMR spectra were fitted by ANATOLIA software [73]. The protons in the  $\text{CH}_3\text{-CH}_2\text{-CH}_2\text{-}$  group were treated as an  $\text{A}_3\text{M}_2\text{X}_2$  system; since the protons in  $\text{CH}_2$  and  $\text{CH}_3$  groups are magnetically equivalent, the coupling within the groups does not influence NMR spectra. The errors in the determinations of the spin-spin couplings are in a range of 0.01-0.05 Hz.

### Chemicals

[U- $^{13}\text{C}$ ,  $^{15}\text{N}$ ]-butyronitrile was obtained from Sigma-Aldrich via custom synthesis, standard iridium precatalyst for SABRE [IrCl(COD)(IMes)] was synthesized as described in [74]. Methanol- $d_4$

(99.8%) was purchased from Carl-Roth (Germany).  $^{14}\text{N}$ -pyridine (99.8%) was purchased from Sigma Aldrich.

## Supporting Information

Details of the numerical simulations, NMR parameters and spectra of bound  $[\text{U-}^{13}\text{C}, ^{15}\text{N}]$ -butyronitrile, as well as experimental details for SABRE generation at hypogeomagnetic fields are provided in the Supplementary Information (SI).

## Acknowledgments

A.K., D.M., I.Z., and A.Y. acknowledges the Ministry of Science and Higher Education of the Russian Federation for granting access to the equipment. D.B. and E.V.D. acknowledge the Alexander von Humboldt Foundation for the financial support provided in the framework of the Sofja Kovalevskaja Award, endowed by the German Federal Ministry of Education and Research.

## Author Contributions

A.K.: data acquisition, methodology, investigation, visualization, writing original draft, review & editing; D.M.: investigation, numerical simulations, visualization, writing original draft, review & editing; I.Z.: investigation, visualization, writing original draft, review & editing; E.V.D.: investigation, review & editing; A.Yu.: review & editing, supervision, resources; D.B.: conceptualization, methodology, investigation, writing original draft, visualization, review & editing, project administration.

## Competing Interests

The authors declare no competing interests.

## References

- [1] Christopher Portmann and Renato Renner. Security in quantum cryptography. *Rev. Mod. Phys.*, 94(2):025008, 2022.
- [2] Charles H Bennett, François Bessette, Gilles Brassard, Louis Salvail, and John Smolin. Experimental quantum cryptography. *J. Cryptol.*, 5(1):3–28, 1992.
- [3] Andrew J Daley, Immanuel Bloch, Christian Kokail, Stuart Flannigan, Natalie Pearson, Matthias Troyer, and Peter Zoller. Practical quantum advantage in quantum simulation. *Nature*, 607(7920):667–676, 2022.
- [4] David P DiVincenzo. The physical implementation of quantum computation. *Fortschr. Phys.*, 48(9-11):771–783, 2000.
- [5] Michael A Nielsen and Isaac L Chuang. *Quantum computation and quantum information*. Cambridge university press, 2010.
- [6] Daniel R Simon. On the power of quantum computation. *SIAM J. Comput.*, 26(5):1474–1483, 1997.

- [7] Jonathan A Jones and Michele Mosca. Implementation of a quantum algorithm on a nuclear magnetic resonance quantum computer. *J. Chem. Phys.*, 109(5):1648–1653, 1998.
- [8] Steffen J Glaser. NMR quantum computing. *Angew. Chem. Int. Ed.*, 40(1):147–149, 2001.
- [9] Noah Linden, Herve Barjat, and Ray Freeman. An implementation of the Deutsch–Jozsa algorithm on a three-qubit nmr quantum computer. *Chem. Phys. Lett.*, 296(1-2):61–67, 1998.
- [10] Isaac L Chuang, Lieven MK Vandersypen, Xinlan Zhou, Debbie W Leung, and Seth Lloyd. Experimental realization of a quantum algorithm. *Nature*, 393(6681):143–146, 1998.
- [11] David G Cory, Amr F Fahmy, and Timothy F Havel. Ensemble quantum computing by NMR spectroscopy. *Proc. Natl. Acad. Sci.*, 94(5):1634–1639, 1997.
- [12] Lieven MK Vandersypen, Matthias Steffen, Gregory Breyta, Costantino S Yannoni, Mark H Sherwood, and Isaac L Chuang. Experimental realization of Shor’s quantum factoring algorithm using nuclear magnetic resonance. *Nature*, 414(6866):883–887, 2001.
- [13] Jonathan A Jones, Michele Mosca, and Rasmus H Hansen. Implementation of a quantum search algorithm on a quantum computer. *Nature*, 393(6683):344–346, 1998.
- [14] Neil A Gershenfeld and Isaac L Chuang. Bulk spin-resonance quantum computation. *Science*, 275(5298):350–356, 1997.
- [15] Michael F O’Keeffe, Lior Horesh, John F Barry, Danielle A Braje, and Isaac L Chuang. Hamiltonian engineering with constrained optimization for quantum sensing and control. *New J. Phys.*, 21(2):023015, 2019.
- [16] Hengyun Zhou, Leigh S Martin, Matthew Tyler, Oksana Makarova, Nathaniel Leitao, Hongkun Park, and Mikhail D Lukin. Robust higher-order Hamiltonian engineering for quantum sensing with strongly interacting systems. *Phys. Rev. Lett.*, 131(22):220803, 2023.
- [17] Hengyun Zhou, Haoyang Gao, Nathaniel T Leitao, Oksana Makarova, Iris Cong, Alexander M Douglas, Leigh S Martin, and Mikhail D Lukin. Robust Hamiltonian engineering for interacting qudit systems. *Phys. Rev. X*, 14(3):031017, 2024.
- [18] Joonhee Choi, Hengyun Zhou, Helena S Knowles, Renate Landig, Soonwon Choi, and Mikhail D Lukin. Robust dynamic Hamiltonian engineering of many-body spin systems. *Phys. Rev. X*, 10(3):031002, 2020.
- [19] Sebastian Geier, Nithiwadee Thaicharoen, Clement Hainaut, Titus Franz, Andre Salzinger, Annika Tebben, David Grimshandl, Gerhard Zürn, and Matthias Weidemüller. Floquet Hamiltonian engineering of an isolated many-body spin system. *Science*, 374(6571):1149–1152, 2021.
- [20] Ashok Ajoy, Rama Koteswara Rao, Anil Kumar, and Pranaw Rungta. Algorithmic approach to simulate Hamiltonian dynamics and an NMR simulation of quantum state transfer. *Phys. Rev. A*, 85(3):030303, 2012.
- [21] Ashok Ajoy and Paola Cappellaro. Quantum simulation via filtered hamiltonian engineering: Application to perfect quantum transport in spin networks. *Phys. Rev. Lett.*, 110(22):220503, 2013.
- [22] William G Alway and Jonathan A Jones. Arbitrary precision composite pulses for NMR quantum computing. *J. Magn. Reson.*, 189(1):114–120, 2007.

- [23] R Marx, AF Fahmy, John M Myers, W Bermel, and SJ Glaser. Approaching five-bit NMR quantum computing. *Phys. Rev. A*, 62(1):012310, 2000.
- [24] Lieven MK Vandersypen and Isaac L Chuang. NMR techniques for quantum control and computation. *Rev. Mod. Phys.*, 76(4):1037–1069, 2004.
- [25] OW Soerensen, GW Eich, Malcolm H Levitt, G Bodenhausen, and RR Ernst. Product operator formalism for the description of NMR pulse experiments. *Prog. Nucl. Magn. Reson. Spectrosc.*, 16:163–192, 1984.
- [26] Alexey Kiryutin, Ivan Zhukov, Danil Markelov, Erik Van Dyke, Alexandra Yurkovskaya, and Danila Barskiy. High-field nmr characterization and indirect j-spectroscopy of a nuclear spin chain [u-13c, 15n]-butyronitrile, 2026.
- [27] Kirill F Sheberstov, Anna Sonnefeld, and Geoffrey Bodenhausen. Collective long-lived zero-quantum coherences in aliphatic chains. *J. Chem. Phys.*, 160(14), 2024.
- [28] Anna Sonnefeld, Aiky Razanahoera, Philippe Pelupessy, Geoffrey Bodenhausen, and Kirill Sheberstov. Long-lived states of methylene protons in achiral molecules. *Sci. Adv.*, 8(48):eade2113, 2022.
- [29] Anna Sonnefeld, Geoffrey Bodenhausen, and Kirill Sheberstov. Polychromatic excitation of delocalized long-lived proton spin states in aliphatic chains. *Phys. Rev. Lett.*, 129(18):183203, 2022.
- [30] Kirill F Sheberstov. Aliphatic chains as one-dimensional XY spin chains. *arXiv preprint*, 2512.23759, 2025.
- [31] Isaac L Chuang, Neil Gershenfeld, Mark G Kubinec, and Debbie W Leung. Bulk quantum computation with nuclear magnetic resonance: theory and experiment. *Proceedings of the Royal Society of London. Series A: Mathematical, Physical and Engineering Sciences*, 454(1969):447–467, 1998.
- [32] Xinhua Peng, Xiwen Zhu, Ximing Fang, Mang Feng, Kelin Gao, Xiaodong Yang, and Maili Liu. Preparation of pseudo-pure states by line-selective pulses in nuclear magnetic resonance. *Chem. Phys. Lett.*, 340(5-6):509–516, 2001.
- [33] Yehuda Sharf, Timothy F Havel, and David G Cory. Spatially encoded pseudopure states for nmr quantum-information processing. *Phys. Rev. A*, 62(5):052314, 2000.
- [34] Marco Pravia, Evan Fortunato, Yaakov Weinstein, Mark D Price, Grum Teklemariam, Richard J Nelson, Yehuda Sharf, Shyamal Somaroo, CH Tseng, Timothy F Havel, et al. Observations of quantum dynamics by solution-state NMR spectroscopy. *Concept. Magn. Reson. A*, 11(4):225–238, 1999.
- [35] Weiyuan Gong, Shuo Zhou, and Tongyang Li. Complexity of digital quantum simulation in the low-energy subspace: Applications and a lower bound. *Quantum*, 8:1409, 2024.
- [36] Warren S. Warren. The usefulness of NMR quantum computing. *Science*, 277(5332):1688–1690, 1997.

- [37] Jan H Ardenkjær-Larsen, Björn Fridlund, Andreas Gram, Georg Hansson, Lennart Hansson, Mathilde H Lerche, Rolf Servin, Mikkel Thaning, and Klaes Golman. Increase in signal-to-noise ratio of  $> 10,000$  times in liquid-state nmr. *Proc. Natl. Acad. Sci.*, 100(18):10158–10163, 2003.
- [38] Peter J Rayner, Michael J Burns, Alexandra M Olaru, Philip Norcott, Marianna Fekete, Gary GR Green, Louise AR Highton, Ryan E Mewis, and Simon B Duckett. Delivering strong  $^1\text{H}$  nuclear hyperpolarization levels and long magnetic lifetimes through signal amplification by reversible exchange. *Proc. Nat. Acad. Sci.*, 114(16):E3188–E3194, 2017.
- [39] Dominic W Berry, Yu Tong, Tanuj Khattar, Alec White, Tae In Kim, Guang Hao Low, Sergio Boixo, Zhiyan Ding, Lin Lin, Seunghoon Lee, et al. Rapid initial-state preparation for the quantum simulation of strongly correlated molecules. *PRX Quantum*, 6(2):020327, 2025.
- [40] Maurice Weber, Abhinav Anand, Alba Cervera-Lierta, Jakob S Kottmann, Thi Ha Kyaw, Bo Li, Alan Aspuru-Guzik, Ce Zhang, and Zhikuan Zhao. Toward reliability in the NISQ era: Robust interval guarantee for quantum measurements on approximate states. *Phys. Rev. Res.*, 4(3):033217, 2022.
- [41] Matthias Rosenkranz, Eric Brunner, Gabriel Marin-Sanchez, Nathan Fitzpatrick, Silas Dilkes, Yao Tang, Yuta Kikuchi, and Marcello Benedetti. Quantum state preparation for multivariate functions. *Quantum*, 9:1703, 2025.
- [42] Jiangfeng Du, Nanyang Xu, Xinhua Peng, Pengfei Wang, Sanfeng Wu, and Dawei Lu. NMR implementation of a molecular hydrogen quantum simulation with adiabatic state preparation. *Phys. Rev. Lett.*, 104(3):030502, 2010.
- [43] C Russell Bowers and Daniel P Weitekamp. Parahydrogen and synthesis allow dramatically enhanced nuclear alignment. *J. Am. Chem. Soc.*, 109(18):5541–5542, 1987.
- [44] MS Anwar, D Blazina, HA Carteret, SB Duckett, and JA Jones. Implementing Grover’s quantum search on a para-hydrogen based pure state NMR quantum computer. *Chem. Phys. Lett.*, 400(1-3):94–97, 2004.
- [45] Damir Blazina, Simon B Duckett, TK Halstead, CM Kozak, RJK Taylor, M Sabieh Anwar, Jonathan A Jones, and Hilary A Carteret. Generation and interrogation of a pure nuclear spin state by parahydrogen-enhanced NMR spectroscopy: a defined initial state for quantum computation. *Magn. Reson. Chem.*, 43(3):200–208, 2005.
- [46] Patrick Hübler, Joachim Bargon, and Steffen J Glaser. Nuclear magnetic resonance quantum computing exploiting the pure spin state of para hydrogen. *J. Chem. Phys.*, 113(6):2056–2059, 2000.
- [47] M Sabieh Anwar, Damir Blazina, Hilary A Carteret, Simon B Duckett, TK Halstead, JA Jones, CM Kozak, and RJK Taylor. Preparing high purity initial states for nuclear magnetic resonance quantum computing. *Phys. Review Lett.*, 93(4):040501, 2004.
- [48] Ralph W Adams, Juan A Aguilar, Kevin D Atkinson, Michael J Cowley, Paul IP Elliott, Simon B Duckett, Gary GR Green, Iman G Khazal, Joaquin Lopez-Serrano, and David C Williamson. Reversible interactions with para-hydrogen enhance NMR sensitivity by polarization transfer. *Science*, 323(5922):1708–1711, 2009.

- [49] Peter J Rayner and Simon B Duckett. Signal amplification by reversible exchange (SABRE): From discovery to diagnosis. *Angew. Chem. Int. Ed.*, 57(23):6742–6753, 2018.
- [50] Thomas Theis, Milton L Truong, Aaron M Coffey, Roman V Shchepin, Kevin W Waddell, Fan Shi, Boyd M Goodson, Warren S Warren, and Eduard Y Chekmenev. Microtesla SABRE enables 10% nitrogen-15 nuclear spin polarization. *J. Am. Chem. Soc.*, 137(4):1404–1407, 2015.
- [51] Milton L Truong, Thomas Theis, Aaron M Coffey, Roman V Shchepin, Kevin W Waddell, Fan Shi, Boyd M Goodson, Warren S Warren, and Eduard Y Chekmenev.  $^{15}\text{N}$  hyperpolarization by reversible exchange using SABRE-SHEATH. *J. Phys. Chem. C*, 119(16):8786–8797, 2015.
- [52] Alexey S Kiryutin, Alexandra V Yurkovskaya, Robert Kaptein, Hans-Martin Vieth, and Konstantin L Ivanov. Evidence for coherent transfer of para-hydrogen-induced polarization at low magnetic fields. *J. Phys. Chem. Lett.*, 4(15):2514–2519, 2013.
- [53] Yuri Alexeev, Marwa H Farag, Taylor L Patti, Mark E Wolf, Natalia Ares, Alan Aspuru-Guzik, Simon C Benjamin, Zhenyu Cai, Shuxiang Cao, Christopher Chamberland, et al. Artificial intelligence for quantum computing. *Nat Commun.*, 16(1):10829, 2025.
- [54] Alexey S Kiryutin, Andrey N Pravdivtsev, Konstantin L Ivanov, Yuri A Grishin, Hans-Martin Vieth, and Alexandra V Yurkovskaya. A fast field-cycling device for high-resolution NMR: Design and application to spin relaxation and hyperpolarization experiments. *J. Magn. Reson.*, 263:79–91, 2016.
- [55] Shannon L Eriksson, Jacob R Lindale, Xiaoqing Li, and Warren S Warren. Improving sabre hyperpolarization with highly nonintuitive pulse sequences: Moving beyond avoided crossings to describe dynamics. *Sci. Adv.*, 8(11):eabl3708, 2022.
- [56] Jacob R Lindale, Loren L Smith, Mathew W Mammen, Shannon L Eriksson, Lucas M Everhart, and Warren S Warren. Multi-axis fields boost sabre hyperpolarization. *Proc. Nat. Acad. Sci.*, 121(14):e2400066121, 2024.
- [57] Vitaly P. Kozinenko, Bogdan A. Rodin, James Eills, Ilai Schwartz, Stephan Knecht, and Laurynas Dagys. Improved SABRE hyperpolarisation using pulse sequences to reduce effective coupling, 2026.
- [58] Michael G Pravica and Daniel P Weitekamp. Net NMR alignment by adiabatic transport of parahydrogen addition products to high magnetic field. *Chem. Phys. Lett.*, 145(4):255–258, 1988.
- [59] Markus Plaumann, Ute Bommerich, Thomas Trantzsche, Denise Lego, Sonja Dillenberger, Grit Sauer, Joachim Bargon, Gerd Buntkowsky, and Johannes Bernarding. Parahydrogen-induced polarization transfer to  $^{19}\text{F}$  in perfluorocarbons for  $^{19}\text{F}$  NMR spectroscopy and MRI. *Chem. Eur. J.*, 19(20):6334–6339, 2013.
- [60] Alexey S. Kiryutin, Vitaly P. Kozinenko, and Alexandra V. Yurkovskaya. Photo-SABRE: Nuclear spin hyperpolarization of cis-trans photoswitchable molecules by parahydrogen. *ChemPhotoChem*, 8(1):e202300151, 2024.
- [61] Malcolm H. Levitt and Christian Bengs. Hyperpolarization and the physical boundary of liouville space. *Magn. Reson.*, 2:395–407, 2021.

- [62] Ole W Sørensen. A universal bound on spin dynamics. *J. Magn. Reson.*, 86(2):435–440, 1990.
- [63] Christian Deppner, Waldemar Herr, Merle Cornelius, Peter Stromberger, Tammo Sternke, Christoph Grzeschik, Alexander Grote, Jan Rudolph, Sven Herrmann, Markus Krutzik, Andre Wenzlawski, Robin Corgier, Eric Charron, David Guery-Odelin, Naceur Gaaloul, Claus Lämmerzahl, Achim Peters, Patrick Windpassinger, and Ernst M. Rasel. Collective-mode enhanced matter-wave optics. *Phys. Rev. Lett.*, 127(10):100401, 2021.
- [64] Martin Schwade, Shaoming Zhang, Frederik Vonhoff, Frederico P Delgado, and David A Egger. Physics-informed hamiltonian learning for large-scale optoelectronic property prediction. *Nat. Commun.*, 2652, 2026.
- [65] Sheng-Hsuan Lin, Rohit Dilip, Andrew G Green, Adam Smith, and Frank Pollmann. Real- and imaginary-time evolution with compressed quantum circuits. *PRX Quantum*, 2(1):010342, 2021.
- [66] Kübra Yeter-Aydeniz, Bryan T. Gard, Jacek Jakowski, Swarnadeep Majumder, George S. Barron, George Siopsis, Travis S. Humble, and Raphael C. Pooser. Benchmarking quantum chemistry computations with variational, imaginary time evolution, and krylov space solver algorithms. *Adv. Quant. Technol.*, 4(7):2100012, 2021.
- [67] Joseph Albert and Robert H. Swendsen. Detecting multi-spin interactions in the inverse ising problem. *Physica A Stat. Mech. Appl.*, 483:293–298, 2017.
- [68] Sylvian Cadars, Julien Sein, Luminita Duma, Anne Lesage, Tran N. Pham, Jay H. Baltisberger, Steven P. Brown, and Lyndon Emsley. The refocused INADEQUATE MAS NMR experiment in multiple spin-systems: Interpreting observed correlation peaks and optimising lineshapes. *J. Magn. Reson.*, 188(1):24–34, 2007.
- [69] Hiroki Ueda, Roman Mankowsky, Eugenio Paris, Mathias Sander, Yunpei Deng, Biaolong Liu, Ludmila Leroy, Abhishek Nag, Elizabeth Skoropata, Chennan Wang, et al. Non-equilibrium dynamics of spin-lattice coupling. *Nat. Commun.*, 14(1):7778, 2023.
- [70] Ivan V Zhukov, Alexey S Kiryutin, Alexandra V Yurkovskaya, Yuri A Grishin, Hans-Martin Vieth, and Konstantin L Ivanov. Field-cycling NMR experiments in an ultra-wide magnetic field range: relaxation and coherent polarization transfer. *Phys. Chem. Chem. Phys.*, 20(18):12396–12405, 2018.
- [71] Alexey S. Kiryutin, Alexandra Yurkovskaya, Herbert Zimmerman, Hans-Martin Vieth, and Konstantin L. Ivanov. Complete magnetic field dependence of SABRE-derived polarization. *Magn. Reson. Chem*, 56(7):651–662, 2018.
- [72] Alexey S. Kiryutin, Grit Sauer, Sara Hadjiali, Alexandra V. Yurkovskaya, Hergen Breitzke, and Gerd Buntkowsky. A highly versatile automatized setup for quantitative measurements of PHIP enhancements. *J. Magn. Reson.*, 285(18):26–36, 2017.
- [73] D.A. Cheshkov, K.F. Sheberstov, D.O. Sinitsyn, and V.A. Chertkov. ANATOLIA: NMR software for spectral analysis of total lineshape. *Magnetic Resonance in Chemistry*, 56(6):449–457, 2018.
- [74] Ireneusz Kownacki, Maciej Kubicki, Karol Szubert, and Bogdan Marciniak. Synthesis, structure and catalytic activity of the first iridium (I) siloxide versus chloride complexes with 1, 3-mesitylimidazol-2-ylidene ligand. *J. of Organomet. Chem.*, 693(2):321–328, 2008.